

Evidence of temperature-dependent interplay between spin and orbital moment in van der Waals ferromagnet VI_3

A. De Vita,^{†,‡,⊥} R. Sant,^{¶,⊥} V. Polewczyk,[‡] G. van der Laan,[§] N. B. Brookes,[¶] T. Kong,^{||} R. J. Cava,^{||} G. Rossi,^{†,‡} G. Vinai,^{*,‡} and G. Panaccione[‡]

[†]*Dipartimento*

di Fisica, Università degli Studi di Milano, Via Celoria 16, I-20133 Milano, Italy

[‡]*Istituto Officina dei Materiali (IOM)-CNR,*

Laboratorio TASC, in Area Science Park, S.S.14, km 163.5, I-34149 Trieste, Italy

[¶]*ESRF, The*

European Synchrotron, 71 Avenue des Martyrs, CS40220, 38043 Grenoble Cedex 9, France

[§]*Diamond Light*

Source, Harwell Science and Innovation Campus, Didcot, Oxfordshire OX11 0DE, UK

^{||}*Department*

of Chemistry, Princeton University, Princeton, New Jersey 08540, United States

[⊥]*These authors contributed equally.*

E-mail: vinai@iom.cnr.it

Abstract

Van der Waals materials provide a versatile toolbox for the emergence of new quantum phenomena and the fabrication of functional heterostructures. Among them, the trihalide VI_3 stands out for its unique magnetic and structural landscape. Here we investigate the spin and orbital magnetic degrees of freedom in the layered ferromagnet VI_3 by means of temperature-dependent x-ray absorption spectroscopy and x-ray magnetic circular and linear dichroism. We detect localized electronic states and reduced magnetic dimensionality, due to electronic correlations. We furthermore provide experimental evidence of (a) an unquenched orbital magnetic moment (up to 0.66(7)) in the ferromagnetic state, and (b) an instability of the orbital moment in proximity of the spin re-orientation transition. Our results support a coherent picture where electronic correlations give rise to a strong magnetic anisotropy and

a large orbital moment, and establish VI_3 as a prime candidate for the study of orbital quantum effects.

Keywords

Van der Waals systems, quantum materials, X-ray absorption spectroscopy, magnetism

Main text

The progress in fundamental research on next-generation magnetic materials is currently spearheaded by two-dimensional (2D) van der Waals (vdW) materials. These compounds have been garnering a large share of attention, as they exhibit a wide array of layer-dependent magnetic ordering;^{1–5} tailoring vdW materials may pave the way for applications in the ever-growing field of spintronics.⁶

Among them, trihalide VI_3 has been exten-

sively studied in the last years.⁷⁻¹³ At variance with the Ising ferromagnet CrI₃, VI₃ is a canted layered ferromagnet with strong magnetocrystalline anisotropy, displaying in its bulk form a structural transition from monoclinic to rhombohedral below $T_s = 79$ K and two ferromagnetic ones, one at the Curie temperature $T_{\text{FM1}} = 50$ K and the other at $T_{\text{FM2}} \approx 35$ K with a variation of spin canting direction and stacking order of layers. The proximity of structural and FM transitions in a narrow temperature interval hints at a relevant interplay between crystal structure and magnetic order. Interestingly, once VI₃ is reduced to few monolayers, T_{FM1} depends on the number of layers;¹⁴ moreover, further clues suggest that VI₃ hosts strong magnetoelastic interactions.¹⁵ The importance of orbital phenomena in solids¹⁶ motivates this line of research on VI₃ also due to its reduced dimensionality. However, to date the understanding of this physics is elusive and mostly limited to magnetometric and structural characterizations.

For this reason, a temperature-dependent spectroscopic investigation of the spin and orbital degrees of freedom is of paramount importance. X-ray magnetic circular dichroism (XMCD) and x-ray natural linear dichroism (XNLD) are ideal techniques for this research. Structural changes influencing the transition metal centres can be monitored by studying the orbital magnetic moment, highly dependent on the local symmetry of the crystal; additionally, the spin magnetic moment reveals the details of the long-range magnetic order, as well as identifying the universality class of the material and its spin dimensionality.

In this Letter, we firstly report the variation of the magnetic and orbital signals in VI₃ crystals, below and above the two FM transitions, by combining XMCD and XNLD measurements. We reveal the presence of a large circular dichroic signal at low temperature, with a clear discontinuity near T_{FM2} and disappearance above T_{FM1} , following a tricritical behavior and compatible with a reduced dimensionality. Linear dichroic measurements disclose a mixed ground state, consistent with a partially unquenched orbital moment supported by clus-

ter calculations, strongly quenched in the proximity of T_{FM2} . Our results confirm the presence of a high orbital moment in VI₃ at low temperature and reveal an orbital instability near T_{FM2} , corroborating the hypothesis of a strong coupling between orbital and magnetic degrees of freedom. These findings underline the relevance of orbital magnetization in VI₃ among vdW crystals and reinforce the importance of quantum spin-orbit entanglement.

The experiment has been performed at the XMCD endstation of the ID32 beamline at the European Synchrotron Radiation Facility (ESRF).^{17,18} Commercially available VI₃ crystals stored in Ar atmosphere (< 0.5 ppm O₂, < 0.5 ppm H₂O) have been transferred in inert static atmosphere and cleaved under N₂ flow inside the loadlock chamber, to expose the (0001) crystallographic plane of the clean surface without contaminating the highly hygroscopic surface; the sample is held in ultra-high vacuum (UHV, pressure $< 3 \times 10^{-10}$ mbar). The structure and 3d electronic configuration of VI₃ are represented in Fig. 1a-b. X-ray absorption spectroscopy (XAS) spectra have been acquired in total electron yield and normalized by the intensity collected on a Au mesh in front of the sample stage. The beam has almost 100% degree of linear and circular polarization, and the setup has resolving power better than 5000. XMCD spectra are the difference between left- and right- circularly polarized light spectra, measured at remanence after zero-field cooling from room temperature to 25 K following application of 0.5 T out-of-plane magnetic field, large enough to saturate the magnetization;⁷ the sample temperature spans the range from 25 K to 65 K. The beam spot diameter at sample position at normal incidence is $100 \mu\text{m} \times 100 \mu\text{m}$. XNLD spectra are the difference between vertically and horizontally polarized light spectra, measured at 20 K, at grazing incidence ($\theta = 70^\circ$) and at remanence. All spectra are normalized by the average of the two light polarizations.

Multiplet cluster calculations have been performed using the *Quanty* code¹⁹ to simulate XNLD signal at 20 K. The trigonal crystal field perturbation has been set to zero, mod-

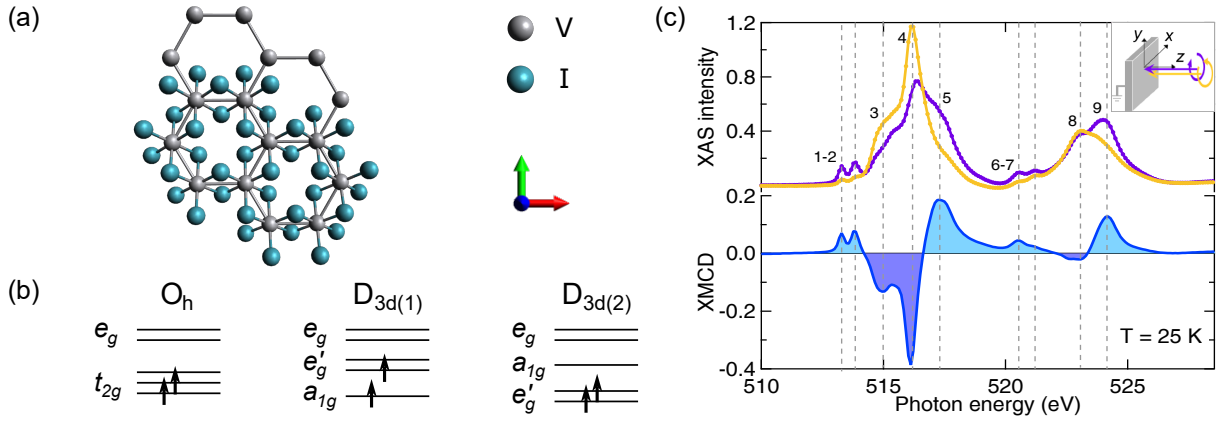


Figure 1: (a) Top pictorial view of a VI_3 layer. Each V centre is coordinated by six I atoms to form VI_6 octahedra. (b) Crystal field splitting and electron filling for O_h and D_{3d} symmetry; in the latter case $3d$ levels are split by elongation (1) or compression (2) along the trigonal axis, resulting in opposite ordering of a_{1g} and e'_g orbitals. (c) *Top*: XAS spectra across the V $L_{2,3}$ edges, acquired with left and right circularly polarized photons at 25 K. The inset shows the experimental geometry. *Bottom*: Corresponding XMCD.

eling instead the trigonal distortion via hybridization potentials $V_{a_{1g}}$ and $V_{e'_g}$. The simulation parameters and the role of trigonal distortion/hybridization in the orbital ordering of VI_3 are discussed in detail elsewhere.²⁰

XAS and XMCD spectra across the V $L_{2,3}$ edges at $T = 25$ K are presented in Fig. 1c. The XAS lineshape shows a complex multiplet structure in agreement with that reported for similarly measured VI_3 spectra, confirming the $3+$ valence state.^{21,22} The L_3 edge is dominated by five spectral features: specifically at 513.3 eV and 513.8 eV (1-2, in the pre-edge region), 515 eV (3), 516.2 eV (4) and 517.3 eV (5). The L_2 peak displays two primary features at 523.1 eV (8) and 524.1 eV (9); between the two edges, the L_2 pre-edge features at 520.5 eV and 521.2 eV (6-7) are the broader counterparts of the (1-2) L_3 pre-edges.

Concerning the XMCD spectrum, the features of L_3 and L_2 edges present both negative (3, 4, 8) and positive (5, 9) dichroism, owing to the combined weak spin-orbit coupling (SOC) and strong hybridization typical in V compounds.²³⁻²⁹ On the other hand, the pre-edge features 1-2 and 6-7, which are associated with transitions from V $2p$ to the unoccupied V $3d t_{2g}^3$ state at the V^{3+} site, present narrow structures, hinting at a localized nature of $3d$ states in the valence band. In the case of L_3 pre-

edges, the XMCD intensity almost corresponds to the intensity of the right circular light, signature of a large asymmetry in the spin population. In addition, both edges exhibit an uncommonly large positive dichroic signal. The positive sign for the L_3 pre-edge, where no shoulder affects the sign of the dichroic signal, is attributed to the final state, *i.e.* an \uparrow electron in the previously partially filled $t_{2g\uparrow}$ states (see Fig. 1b), to which a corresponding negative one would be expected for the L_2 pre-edge.²⁵ We attribute this lack in inversion to the large degree of hybridization of V^{3+} in the crystal: indeed, the long tail of the L_3 main peak at ~ 517 eV (5) extends up to the L_2 pre-edge region, shadowing the sign reversal of the pre-edge peak.

The large dichroic signal on the L_3 main peak (≈ 0.4) is a clear indication of FM ordering. In order to study the dependence of the magnetic character on temperature, we performed the same measurements while raising the temperature up to above T_{FM1} , which are plotted in Fig. 2a-b. The temperature increase produces no qualitative modification in the features of both XAS and XMCD spectra. The XMCD lineshape reported in Fig. 2b shows that magnetic order is preserved up to 51 K, whereas from 53 K onward the signal intensity becomes comparable with the sensitivity limit of the beamline, losing information on the de-

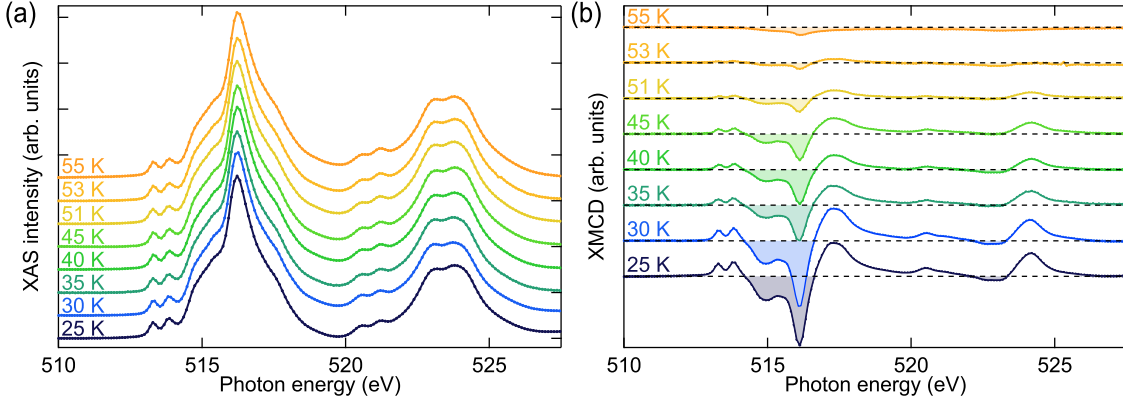


Figure 2: (a) XAS average spectra across the V $L_{2,3}$ edges as a function of temperature. (b) Corresponding XMCD.

tails of the overall spectrum. This indicates that the Curie temperature lies between 51 K and 53 K, in agreement with literature.^{7–9,30}

The XMCD signal allows an element-sensitive quantitative evaluation on the magnetic spin and orbital moments via sum rules analysis.³¹ However, calculations of the spin moment contribution become inadequate for early transition metals, where the large overlap between L_3 and L_2 edges prevents a clear-cut distinction.³² Therefore, we follow the evolution of VI_3 magnetic character by plotting the XMCD intensity at the L_3 main peak, as displayed in Fig. 3. A first observation is the abrupt reduction of the signal between 30 K and 35 K. This discontinuity may be explained in terms of the nature of the FM transition. In previous studies³⁰ a weak discontinuity of the heat capacity appears at $T_{\text{FM}2}$: additionally, since a second-order transition takes place at $T_{\text{FM}1}$, thermodynamic considerations prevent the one at $T_{\text{FM}2}$ to display a second-order character.³³ We thus infer that a weak first-order transition at this temperature would result in a discontinuity of the order parameter. Moreover, a structural transition from triclinic to monoclinic has been reported at $T_{\text{FM}2}$, together with an in-plane rotation of the canted V spins;^{15,34,35} this could justify the variation of dichroic signal below $T_{\text{FM}2}$, as the concurrent change of crystal structure and magnetic easy axis could modify the projection of the magnetic moment along the out-of-plane direction.

Around $T_{\text{FM}1}$, the trend of the XMCD signal

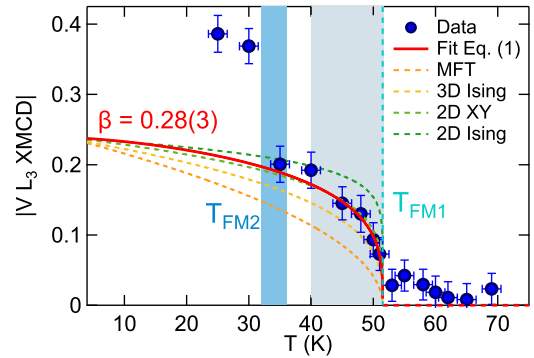


Figure 3: XMCD maximal intensity at the V L_3 edge as a function of temperature, and visual comparison with theoretical models. The solid red line plots the fit following Eq. 1, in the temperature range highlighted by the gray area; dotted lines trace curves for mean field ($\beta = 0.5$), 3D Ising ($\beta = 0.33$), 2D XY ($\beta = 0.23$) and 2D Ising ($\beta = 0.125$) models. The teal dotted line marks $T_{\text{FM}1}$ as retrieved from the fit, the light blue shaded area indicates $T_{\text{FM}2}$.

can be assessed in order to extract information on the spin dimensionality. To do so, we fitted the curve in Fig. 3 with the Curie-Weiss law

$$m \sim (\tau)^\beta, \quad (1)$$

where $\tau = (T_{\text{FM1}} - T)/T_{\text{FM1}}$, and β and T_{FM1} are free parameters of the fit. The procedure has been performed for $\tau \leq 0.1$, *i.e.* in a region close to the transition, to ensure the validity of the formula. The fit yields values of $T_{\text{FM1}} = 51.5(5)$ K and $\beta = 0.28(3)$. The critical exponent β governing the order parameter gives indications on the universality class of the material, being $\beta = 0.23$ for dimensionality $n = 2$ and $\beta = 0.5$ for dimensionality $n = 3$ (*cf.* the dotted curves exemplifying different models in Fig. 3). Our results suggest that VI_3 magnetic character is denoted by a reduced spin dimensionality, as expected for a quasi-2D crystal with weak inter-plane interactions,³⁶ in agreement with what found on other vdW materials^{37–39} and by magnetometric measurements on VI_3 .^{14,40}

The extracted value of β and the first-order FM transition at T_{FM2} point at the tricritical mean field model as a good description of the critical behavior of VI_3 . In the VI_3 $p - T$ phase diagram,³⁰ the two FM transitions merge at a triple point (p_{c1}, T_{c1}) with increasing pressure: our measurements further support the hypothesis that this is also a tricritical point.

In addition to XMCD, we performed XNLD on V $L_{2,3}$ edges to retrieve information on the orbital ordering. We showed that the pre-edge features previously identified (Fig. 1 and discussion) result from transitions to unoccupied t_{2g} states; in particular, the trigonal distortion splits the t_{2g} level into a_{1g} and e'_g , with mostly out-of-plane and in-plane character respectively. In an XNLD experiment with grazing angle geometry, horizontally (vertically) polarized photons interact mostly with out-of-plane (in-plane) orbitals: it is thus possible to discern which level is occupied from the change in the spectral weight of the pre-edge features.

XAS spectra acquired with linearly polarized light, and the corresponding XNLD, are displayed in Fig. 4. We reveal a negative dichro-

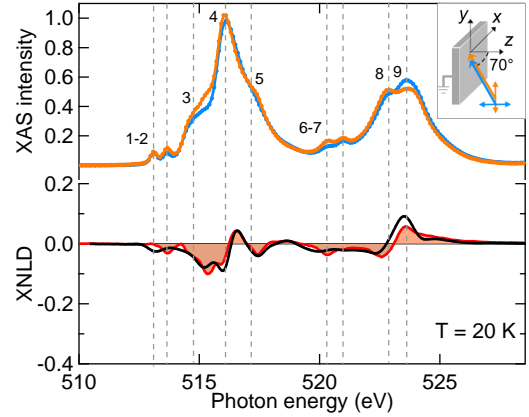


Figure 4: *Top*: XAS spectra across the V $L_{2,3}$ edges, acquired with linearly polarized photons at 20 K. The inset shows the experimental geometry. *Bottom*: calculated (solid black line) and measured (red shaded area) XNLD.

ism in both pre-edge regions (1-2 and 6-7): the signal derived from the excitation induced by linear light polarization vector $E \perp c$ (vertical polarization) is enhanced compared to $E \parallel c$ (horizontal polarization), consistently with the XNLD reported by our group.²⁰ By means of cluster calculations, the XNLD at 20 K is simulated in the framework of the ligand-field multiplet theory. In Fig. 4, the resulting curve (solid black line) obtained with hybridization parameters $V_{a_{1g}} = 1.097$ eV and $V_{e'_g} = 1.103$ eV is in excellent agreement with experimental data, indicating an $a_{1g}^1 e'_g{}^1$ ground state. Furthermore, as a comparison with a similar V^{3+} system, in V_2O_3 the pre-edge intensity increases when the a_{1g} orbital is unoccupied and $E \parallel c$.⁴¹ Our observation suggests that in the initial state the a_{1g} orbital is filled: this is also in agreement with a recent ARPES characterization, where the a_{1g} orbital lies at the top of the valence band and displays strong photoemission intensity,²¹ and with the large orbital moment measured by Hovancik et al.²² We note however that the resulting linear dichroism is quite small compared to e.g. the one calculated for V_2O_3 , indicating that the energy difference between $e'_g{}^2$ and $a_{1g}^1 e'_g{}^1$ ground states is small, and tiny lattice distortions and/or partial charge transfer could stabilize a mixed electronic configuration.²⁰

The stabilization of an $a_{1g}^1 e'_g{}^1$ ground state

drives the appearance of a high orbital moment in FM VI_3 . To assess the effect of temperature, we calculated the orbital moment from XMCD data displayed in Fig. 2 by applying the orbital sum rule,³¹ as shown in Fig. 5. The value at 25 K ($L_z = 0.66(7)$) is comparable with the other reported result²² for a 50% occupancy of each possible ground state ($e'_g{}^2$ and $a_{1g}^1 e'_g{}^1$). However, as the temperature increases we notice a strong quenching of the orbital moment at 40 K, which then recovers and gradually goes to zero close to T_{FM1} . If we consider that T_{FM2} lies between 32 K and 36 K,^{15,30,42,43} the proximity of the sharp disruption of the orbital moment to T_{FM2} indicates a connection to the critical dynamics of the transition: the orbital instability is indeed a signature of a change in the anisotropy constant of the lattice,⁴⁴ and has been demonstrated to be a precursor of spin reorientation transitions.⁴⁵ Changes in the magnetic anisotropy accompanied by a spin reorientation have also been reported in other vdW materials exhibiting a similar magnetic anisotropy, such as Fe_4GeTe_2 .^{13,46}

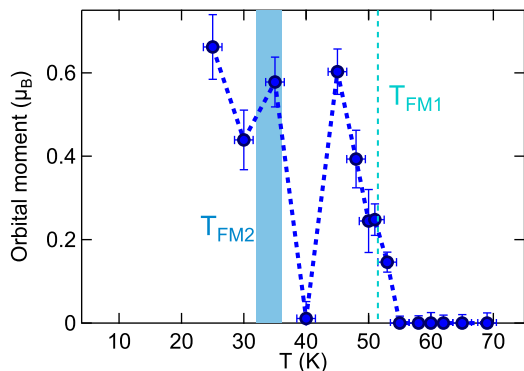


Figure 5: Orbital magnetic moment on V^{3+} as a function of temperature. The green dotted line and the teal shaded area indicate the two FM transition temperatures.

The presence of an unquenched orbital moment has deep implications in the physics of low-dimensional materials. $3d$ transition metals display quenched orbital moment and weak SOC (in the order of few tens of millielectronvolts); however, strong SOC may appear when electron correlations lead to a spin-entangled state, as suggested in the Ising metallic system

$\text{Fe}_{1/4}\text{TaS}_2$,⁴⁷ or recently in the 2D vdW anti-ferromagnet FePS_3 ,⁴⁸ where large orbital moment and SOC ultimately give rise to a sizeable magnetic anisotropy. VI_3 , a system with a large unquenched moment where SOC cannot be neglected without hampering the interpretation of experimental spectra,²¹ has been proposed as a candidate material where electronic correlations enhance the orbital magnetization.⁴⁹ Therefore, future efforts to understand the microscopic origin of the large magnetic anisotropy in VI_3 should focus on the orbital degree of freedom, in view of spintronics applications.

In summary, in this work we present and interpret temperature-dependent XMCD measurements, with the support of XNLD and cluster calculations, to assess the spin and orbital degrees of freedom in VI_3 . XMCD reveals a magnetic state with strong (up to ≈ 0.4) dichroism, whose lineshape is not qualitatively affected by temperature, and well-defined pre-edge features, signature of localized states.

The XMCD maximal intensity at the L_3 edge shows an abrupt decrease at the first-order FM transition at T_{FM2} , and displays a critical behavior following an exponent $\beta = 0.28(3)$, suggesting a tricritical mean field model and a reduced dimensionality.

The XNLD spectrum exhibits a sizeable negative linear dichroism on the pre-edges, implying an at least partially filled a_{1g} orbital in the ground state and non-zero orbital moment: further analysis from temperature-dependent XMCD spectra confirm a large (up to $L_z = 0.66(7)$) orbital moment, and unveil the presence of a large orbital instability near T_{FM2} . This is interpreted in terms of changes in the magnetic anisotropy of the crystal, disrupting the orbital moment and kickstarting the subsequent spin reorientation. Our study demonstrates that VI_3 hosts exotic quantum properties and will bolster advanced investigations into vdW 2D ferromagnets.

Acknowledgments

We acknowledge the European Synchrotron Radiation Facility for provision of beamtime on the ID32 beamline. G.P. acknowledges financial support from PNRR MUR project PE0000023-NQSTI. This work has been performed in the framework of the Nanoscience Foundry and Fine Analysis (NFFA-MUR Italy Progetti Internazionali) project (www.trieste.NFFA.eu).

Author Contributions

A.D.V., R.S., G.V. and G.P. designed the research; A.D.V., R.S., V.P., N.B. and G.V. performed the experiment; A.D.V. and G.V. analyzed data; R.S. and G.v.d.L. performed the simulations; R.J.C. and T.K. provided samples for early measurements; G.R. and G.P. provided support with funding and supervision; A.D.V. and G.V. wrote the paper with contributions from all authors. All authors have given approval to the final version of the manuscript.

A.D.V. and R.S. equally contributed to this work.

References

- (1) Butler, S. et al. Progress, challenges, and opportunities in two-dimensional materials beyond graphene. *ACS Nano* **2013**, *7*, 2898–2926.
- (2) Samarth, N. Magnetism in flatland. *Nature* **2017**, *546*, 216–217.
- (3) Mounet, N.; Gibertini, M.; Schwaller, P.; Campi, D.; Merkys, A.; Marrazzo, A.; Sohler, T.; Castelli, I.; Cepellotti, A.; Pizzi, G.; Marzari, N. Two-dimensional materials from high-throughput computational exfoliation of experimentally known compounds. *Nat. Nanotechnol.* **2018**, *13*, 246–252.
- (4) Burch, K. S.; Mandrus, D.; Park, J.-G. Magnetism in two-dimensional van der Waals materials. *Nature* **2018**, *563*, 47–52.
- (5) Gibertini, M.; Koperski, M.; Morpurgo, A.; Novoselov, K. Magnetic 2D materials and heterostructures. *Nat. Nanotechnol.* **2019**, *14*, 408–419.
- (6) Disa, A. S.; Nova, T. F.; Cavalleri, A. Engineering crystal structures with light. *Nature Physics* **2021**, *17*, 1087–1092.
- (7) Son, S.; Coak, M. J.; Lee, N.; Kim, J.; Kim, T. Y.; Hamidov, H.; Cho, H.; Liu, C.; Jarvis, D. M.; Brown, P. A. C.; Kim, J. H.; Park, C.-H.; Khomskii, D. I.; Saxena, S. S.; Park, J.-G. Bulk properties of the van der Waals hard ferromagnet VI_3 . *Phys. Rev. B* **2019**, *99*, 041402.
- (8) Tian, S.; Zhang, J.-F.; Li, C.; Ying, T.; Li, S.; Zhang, X.; Liu, K.; Lei, H. Ferromagnetic van der Waals Crystal VI_3 . *Journal of the American Chemical Society* **2019**, *141*, 5326–5333.
- (9) Kong, T.; Stolze, K.; Timmons, E. I.; Tao, J.; Ni, D.; Guo, S.; Yang, Z.; Prozorov, R.; Cava, R. J. VI_3 – a New Layered Ferromagnetic Semiconductor. *Advanced Materials* **2019**, *31*, 1808074.
- (10) Yang, K.; Fan, F.; Wang, H.; Khomskii, D. I.; Wu, H. VI_3 : A two-dimensional Ising ferromagnet. *Phys. Rev. B* **2020**, *101*, 100402.
- (11) Zhang, X.; Wang, L.; Su, H.; Xia, X.; Liu, C.; Lyu, B.; Lin, J.; Huang, M.; Cheng, Y.; Mei, J.-W.; Dai, J.-F. Strain Tunability of Perpendicular Magnetic Anisotropy in van der Waals Ferromagnets VI_3 . *Nano Letters* **2022**, *22*, 9891–9899.
- (12) Bergner, D.; Kong, T.; Ai, P.; Eilbott, D.; Fatuzzo, C.; Ciocys, S.; Dale, N.; Stansbury, C.; Latzke, D. W.; Molina, E.; Reno, R.; Cava, R. J.; Lanzara, A.; Ojeda-Aristizabal, C. Polarization dependent photoemission as a probe of the magnetic ground state in the van der Waals ferromagnet VI_3 . *Applied Physics Letters* **2022**, *121*, 183104.

- (13) Wang, W.; Sun, R.; Shen, W.; Jia, Z.; Deepak, F. L.; Zhang, Y.; Wang, Z. Atomic structure and large magnetic anisotropy in air-sensitive layered ferromagnetic VI₃. *Nanoscale* **2023**, *15*, 4628–4635.
- (14) Lin, Z.; Huang, B.; Hwangbo, K.; Jiang, Q.; Zhang, Q.; Liu, Z.; Fei, Z.; Lv, H.; Millis, A.; McGuire, M.; Xiao, D.; Chu, J.-H.; Xu, X. Magnetism and Its Structural Coupling Effects in 2D Ising Ferromagnetic Insulator VI₃. *Nano Letters* **2021**, *21*, 9180–9186.
- (15) Doležal, P.; Kratochvílová, M.; Holý, V.; Čermák, P.; Sechovský, V.; Dušek, M.; Míšek, M.; Chakraborty, T.; Noda, Y.; Son, S.; Park, J.-G. Crystal structures and phase transitions of the van der Waals ferromagnet VI₃. *Phys. Rev. Mater.* **2019**, *3*, 121401.
- (16) Khomskii, D. I.; Streltsov, S. V. Orbital Effects in Solids: Basics, Recent Progress, and Opportunities. *Chemical Reviews* **2021**, *121*, 2992–3030.
- (17) Kummer, K.; Fondacaro, A.; Jimenez, E.; Velez-Fort, E.; Amorese, A.; Aspbury, M.; Yakhou-Harris, F.; van der Linden, P.; Brookes, N. B. The high-field magnet endstation for X-ray magnetic dichroism experiments at ESRF soft X-ray beamline ID32. *Journal of Synchrotron Radiation* **2016**, *23*, 464–473.
- (18) Brookes, N. B. et al. The beamline ID32 at the ESRF for soft X-ray high energy resolution resonant inelastic X-ray scattering and polarisation dependent X-ray absorption spectroscopy. *Nuclear Instruments and Methods in Physics Research Section A: Accelerators, Spectrometers, Detectors and Associated Equipment* **2018**, *903*, 175–192.
- (19) Haverkort, M. W. Quanta for core level spectroscopy - excitons, resonances and band excitations in time and frequency domain. *Journal of Physics: Conference Series* **2016**, *712*, 012001.
- (20) Sant, R.; De Vita, A.; Polewczyk, V.; Pierantozzi, G.; Mazzola, F.; Vinai, G.; van der Laan, G.; Panaccione, G.; Brookes, N. Anisotropic hybridization probed by polarization dependent x-ray absorption spectroscopy in VI₃ van der Waals Mott ferromagnet. *Journal of Physics: Condensed Matter* **2023**, *35*, 405601.
- (21) De Vita, A. et al. Influence of Orbital Character on the Ground State Electronic Properties in the van Der Waals Transition Metal Iodides VI₃ and CrI₃. *Nano Letters* **2022**, *22*, 7034–7041.
- (22) Hovančík, D.; Pospíšil, J.; Carva, K.; Sechovský, V.; Piamonteze, C. Large Orbital Magnetic Moment in VI₃. *Nano Letters* **2023**, *23*, 1175–1180.
- (23) de Groot, F. M. F.; Fuggle, J. C.; Thole, B. T.; Sawatzky, G. A. 2p x-ray absorption of 3d transition-metal compounds: An atomic multiplet description including the crystal field. *Phys. Rev. B* **1990**, *42*, 5459–5468.
- (24) Abbate, M.; Pen, H.; Czyżyk, M.; de Groot, F.; Fuggle, J.; Ma, Y.; Chen, C.; Sette, F.; Fujimori, A.; Ueda, Y.; Kosuge, K. Soft X-ray absorption spectroscopy of vanadium oxides. *Journal of Electron Spectroscopy and Related Phenomena* **1993**, *62*, 185–195.
- (25) Matsuura, K.; Sagayama, H.; Nii, Y.; Khanh, N. D.; Abe, N.; Arima, T. X-ray magnetic circular dichroism study of an orbital ordered state in the spinel-type vanadium oxide AV₂O₄ (A = Mn, Fe). *Phys. Rev. B* **2015**, *92*, 035133.
- (26) Zhang, W.; Zhang, L.; Wong, P. K. J.; Yuan, J.; Vinai, G.; Torelli, P.; van der

- Laan, G.; Feng, Y. P.; Wee, A. T. S. Magnetic Transition in Monolayer VSe₂ via Interface Hybridization. *ACS Nano* **2019**, *13*, 8997–9004.
- (27) Vinai, G.; Bigi, C.; Rajan, A.; Watson, M. D.; Lee, T.-L.; Mazzola, F.; Modesti, S.; Barua, S.; Ciomaga Hatnean, M.; Balakrishnan, G.; King, P. D. C.; Torelli, P.; Rossi, G.; Panaccione, G. Proximity-induced ferromagnetism and chemical reactivity in few-layer VSe₂ heterostructures. *Phys. Rev. B* **2020**, *101*, 035404.
- (28) Schmitz, D.; Schmitz-Antoniak, C.; Radu, F.; Ryll, H.; Luo, C.; Bhandary, S.; Biermann, S.; Siemsmeyer, K.; Wende, H.; Ivanov, S.; Eriksson, O. Soft X-Ray Magnetic Circular Dichroism of Vanadium in the Metal–Insulator Two-Phase Region of Paramagnetic V₂O₃ Doped with 1.1% Chromium. *Phys. Status Solidi B* **2020**, *257*, 1900456.
- (29) Maganas, D.; Kowalska, J. K.; Van Stappen, C.; DeBeer, S.; Neese, F. Mechanism of L_{2,3}-edge x-ray magnetic circular dichroism intensity from quantum chemical calculations and experiment—A case study on V(IV)/V(III) complexes. *The Journal of Chemical Physics* **2020**, *152*, 114107.
- (30) Gati, E.; Inagaki, Y.; Kong, T.; Cava, R. J.; Furukawa, Y.; Canfield, P. C.; Bud’ko, S. L. Multiple ferromagnetic transitions and structural distortion in the van der Waals ferromagnet VI₃ at ambient and finite pressures. *Phys. Rev. B* **2019**, *100*, 094408.
- (31) Chen, C. T.; Idzerda, Y. U.; Lin, H.-J.; Smith, N. V.; Meigs, G.; Chaban, E.; Ho, G. H.; Pellegrin, E.; Sette, F. Experimental Confirmation of the X-Ray Magnetic Circular Dichroism Sum Rules for Iron and Cobalt. *Phys. Rev. Lett.* **1995**, *75*, 152–155.
- (32) O’Brien, W. L.; Tonner, B. P.; Harp, G. R.; Parkin, S. S. P. Experimental investigation of dichroism sum rules for V, Cr, Mn, Fe, Co, and Ni: Influence of diffuse magnetism. *Journal of Applied Physics* **1994**, *76*, 6462–6464.
- (33) Yip, S. K.; Li, T.; Kumar, P. Thermodynamic considerations and the phase diagram of superconducting UPt₃. *Phys. Rev. B* **1991**, *43*, 2742–2747.
- (34) Koriki, A.; Míšek, M.; Pospíšil, J.; Kratochvílová, M.; Carva, K.; Prokleška, J.; Doležal, P.; Kaštil, J.; Son, S.; Park, J.-G.; Sechovský, V. Magnetic anisotropy in the van der Waals ferromagnet VI₃. *Phys. Rev. B* **2021**, *103*, 174401.
- (35) Hao, Y.; Gu, Y.; Gu, Y.; Feng, E.; Cao, H.; Chi, S.; Wu, H.; Zhao, J. Magnetic Order and Its Interplay with Structure Phase Transition in van der Waals Ferromagnet VI₃. *Chinese Physics Letters* **2021**, *38*, 096101.
- (36) Taroni, A.; Bramwell, S. T.; Holdsworth, P. C. W. Universal window for two-dimensional critical exponents. *Journal of Physics: Condensed Matter* **2008**, *20*, 275233.
- (37) Zaiyao, F.; Bevin, H.; Paul, M.; Wenbo, W.; Tiancheng, S.; Joshua, S.; Wang, Y.; Di, X.; Xiaoyang, Z.; F., M. A.; Weida, W.; H., C. D.; Jiun-Haw, C.; Xiaodong, X. Two-dimensional itinerant ferromagnetism in atomically thin Fe₃GeTe₂. *Nature Mater.* **2018**, *17*, 778–782.
- (38) Bedoya-Pinto, A.; Ji, J.-R.; Pandeya, A. K.; Gargiani, P.; Valvidares, M.; Sessi, P.; Taylor, J. M.; Radu, F.; Chang, K.; Parkin, S. S. P. Intrinsic 2D-XY ferromagnetism in a van der Waals monolayer. *Science* **2021**, *374*, 616–620.
- (39) Wildes, A. R.; Rønnow, H. M.; Roessli, B.; Harris, M. J.; Godfrey, K. W. Static and

- dynamic critical properties of the quasi-two-dimensional antiferromagnet MnPS_3 . *Phys. Rev. B* **2006**, *74*, 094422.
- (40) Liu, Y.; Abeykoon, M.; Petrovic, C. Critical behavior and magnetocaloric effect in VI_3 . *Phys. Rev. Res.* **2020**, *2*, 013013.
- (41) Park, J.-H.; Tjeng, L. H.; Tanaka, A.; Allen, J. W.; Chen, C. T.; Metcalf, P.; Honig, J. M.; de Groot, F. M. F.; Sawatzky, G. A. Spin and orbital occupation and phase transitions in V_2O_3 . *Phys. Rev. B* **2000**, *61*, 11506–11509.
- (42) Marchandier, T.; Dubouis, N.; Fauth, F. m. c.; Avdeev, M.; Grimaud, A.; Tarascon, J.-M.; Rousse, G. Crystallographic and magnetic structures of the VI_3 and LiVI_3 van der Waals compounds. *Phys. Rev. B* **2021**, *104*, 014105.
- (43) Soler-Delgado, D.; Yao, F.; Dumcenco, D.; Giannini, E.; Li, J.; Occhialini, C. A.; Comin, R.; Ubrig, N.; Morpurgo, A. F. Probing Magnetism in Exfoliated VI_3 Layers with Magnetotransport. *Nano Letters* **2022**, *22*, 6149–6155.
- (44) García, L. M.; Chaboy, J.; Bartolomé, F.; Goedkoop, J. B. Orbital Magnetic Moment Instability at the Spin Reorientation Transition of $\text{Nd}_2\text{Fe}_{14}\text{B}$. *Phys. Rev. Lett.* **2000**, *85*, 429–432.
- (45) Removic-Langer, K.; Hunter Dunn, J.; Langer, J.; Arvanitis, D.; Maletta, H.; Holub-Krappe, E. Spin and orbital moments in $\text{Au/Co/Au(111)/W(110)}$ across the spin-reorientation transition-temperature. *Nuclear Instruments and Methods in Physics Research Section B: Beam Interactions with Materials and Atoms* **2003**, *200*, 210–214, Proceedings of the E-MRS 2002 Symposium I on Synchrotron Radiation and Materials Science.
- (46) Seo, J. et al. Nearly room temperature ferromagnetism in a magnetic metal-rich van der Waals metal. *Science Advances* **2020**, *6*, eaay8912.
- (47) Ko, K.-T.; Kim, K.; Kim, S. B.; Kim, H.-D.; Kim, J.-Y.; Min, B. I.; Park, J.-H.; Chang, F.-H.; Lin, H.-J.; Tanaka, A.; Cheong, S.-W. RKKY Ferromagnetism with Ising-Like Spin States in Intercalated $\text{Fe}_{1/4}\text{TaS}_2$. *Phys. Rev. Lett.* **2011**, *107*, 247201.
- (48) Lee, Y. et al. Giant Magnetic Anisotropy in the Atomically Thin van der Waals Antiferromagnet FePS_3 . *Advanced Electronic Materials* **2023**, *9*, 2200650.
- (49) Zhou, Z.; Pandey, S. K.; Feng, J. Dynamical correlation enhanced orbital magnetization in VI_3 . *Phys. Rev. B* **2021**, *103*, 035137.